Geomechanics and Engineering, Vol. 2, No. 2 (2010) 89-106
DOI: http://dx.doi.org/10.12989/gae.2010.2.2.089

Physical modelling of sliding failure of concrete gravity dam under overloading condition

Hong-Hu Zhu[1], *Jian-Hua Yin[1,2], Jian-Hua Dong[2,3] and Lin Zhang[2,3]

[1]*Department of Civil and Structural Engineering, The Hong Kong Polytechnic University, Hung Hom, Kowloon, Hong Kong, China*
[2]*State Key Laboratory of Hydraulics and Mountain River Engineering, Sichuan University, Chengdu, Sichuan, China*
[3]*School of Water Resources and Hydropower Engineering, Sichuan University, Chengdu, Sichuan, China*

(Received September 10, 2009, Accepted March 19, 2010)

Abstract. Sliding within the dam foundation is one of the key failure modes of a gravity dam. A two-dimensional (2-D) physical model test has been conducted to study the sliding failure of a concrete gravity dam under overloading conditions. This model dam was instrumented with strain rosettes, linear variable displacement transformers (LVDTs), and embedded fiber Bragg grating (FBG) sensing bars. The surface and internal displacements of the dam structure and the strain distributions on the dam body were measured with high accuracy. The setup of the model with instrumentation is described and the monitoring data are presented and analyzed in this paper. The deformation process and failure mechanism of dam sliding within the rock foundation are investigated based on the test results. It is found that the horizontal displacements at the toe and heel indicate the dam stability condition. During overloading, the cracking zone in the foundation can be simplified as a triangle with gradually increased height and vertex angle.

Keywords: concrete gravity dam; rock foundation; overloading; physical model test; sliding failure; fiber Bragg grating (FBG).

1. Introduction

In the past two decades, a number of massive concrete gravity dams have been or are being constructed in China, such as the Longtan Dam (maximum height H=216.5m) (Zhang *et al.* 2002), the Three-Gorges Dam (H=185m) (Liu *et al.* 2003a and 2003b, Li *et al.* 2005), the Xiangjiaba Dam (H=161m) (Zhou *et al.* 2008), the Jiangya Dam (H=131m) (Yan *et al.* 2004), the Baise Dam (H=130m) (Xu *et al.* 2007), and the Baozhusi Dam (H=131m) (Chen *et al.* 2004, 2008). In harsh conditions such as flooding and earthquake, dam safety becomes an issue of great concern.

The gravity dam is a high order statically indeterminate structure and the dam stability relies mainly on its self-weight. The field performance of the dam is affected by its surrounding environments, including hydrological and meteorological factors, reservoir rim, and seismic loading (ASCE Task Committee on Instrumentation and Monitoring Dam Performance 2000). Gravity dams are always

*Corresponding author, Professor, E-mail: cejhyin@polyu.edu.hk

required to be in the elastic state under working conditions and have adequate resistance to failure. The failure modes of concrete gravity dams can be grouped into three categories, namely overturning, cracking, and sliding (U.S. Army Corps of Engineers 1995). Given appropriate structural design, the overturning failure can be avoided. The cracking of concrete is a critical factor affecting the dam stability. This phenomenon has been extensively examined (Donlon and Hall 1991, Bhattacharjee and Léger 1993 and 1994, Tinawi and Guizani 1994, Plizzari *et al.* 1995, Mao and Taylor 1997, Ghaemina and Ghobarah 1999, Barpi *et al.* 1999, Harris *et al.* 2000, Tinawi *et al.* 2000, Javanmardi *et al.* 2005, Ftima and Léger 2006, Zhu and Pekau 2007) and various reinforcement techniques have been successfully utilized (Morin *et al.* 2002). The sliding can occur at the concrete-rock interface or within the rock foundation. Chopra and Zhang (1991) studied earthquake-induced sliding of a gravity dam monolith supported without bond on a horizontal, planar surface of rock and tried to calculate the sliding displacements. Mir and Taylor (1996) studied the base sliding response of rigid concrete gravity dams subjected to dynamic loading. Rochon-Cyr and Léger (2009) performed shake table tests to study the sliding response of a gravity dam model including water uplift pressure. For dams on jointed and decomposed rock masses, or even soils with low shear strength and high compressibility, the failure of the dam-foundation system frequently occurred within the foundation instead of the concrete-rock interface (Liu *et al.* 2003a, 2003b, Zhou *et al.* 2008, Barpi *et al.* 1999, Martt *et al.* 2005, Ren *et al.* 2008). This kind of deformation process and sliding mechanism is not well defined in previous studies.

The evaluation of performance and safety of a high gravity dam under overloading conditions has attracted wide attention in the field of dam engineering (Liu *et al.* 2003a and 2003b, Chen *et al.* 2004 and 2008, Ghaemina and Ghobarah 1999, Alonso *et al.* 1996). If the horizontal component of hydrostatic pressure on the upstream face is increased above the design value, the limiting state of the dam stability can be achieved, where the carrying capacity of the dam is fully exhausted. This makes it possible to investigate the dam failure mode under external overloading, considering the uncertainties of the upstream hydrostatic load. In this regard, the factor of safety of a gravity dam can be defined as the ratio of the maximum external load inducing the start of sliding instability to the applied upstream hydrostatic load. There are mainly three approaches to study the overloaded dam performance, i.e., limit equilibrium method, physical modelling, and numerical simulation. The limit-equilibrium method is not suitable for complex structure-foundation systems (U.S. Army Corps of Engineers 1995). Considerations regarding displacements are excluded in this method. In previous researches of numerical analysis, the deformation pattern and failure mechanism of a high gravity dam system under staged overloading cannot be fully identified because of the simplification of constitutive models and geological conditions. Physical model testing provides a visible and comprehensive interpretation of the dam performance under various loading combinations. The current design specifications in China recommend using physical modelling for dams with complicated foundation conditions (The State Economic and Trade Commission 2000, Ministry of Water Resources 2005). Due to the constraint of experimental techniques, some difficulties were encountered, such as simulating actual hydraulic conditions and obtaining reliable monitoring results with high accuracy (Liu *et al.* 2003a, Plizzari *et al.* 1995, Ghobarah and Ghaemian 1998).

This study was carried out to analyze the deformation process of the dam-foundation system under progressive overloading, with a particular focus on the sliding failure mechanism within the dam foundation. This issue was investigated through a laboratory physical model test with improved measurement technologies. Based on the test results, the potential sliding path of high gravity dams under overloading condition was further discussed.

2. Test setup and procedure

The dam investigated in the physical model test is a concrete gravity dam structure with a height of 75 m and a downstream slope of 0.8. The dam was built on a rock foundation along its bottom-line. A two-dimensional (2-D) model was constructed and tested in the School of Water Resources and Hydropower Engineering, Sichuan University. The geometry of the model dam is shown in Fig. 1.

According to similarity theory of physical modelling, the following similarity criteria must be met

$$\frac{C_\sigma}{C_\gamma C_L} = 1 \tag{1}$$

$$C_\varepsilon = C_\gamma = C_\nu = 1 \tag{2}$$

$$\frac{C_\sigma}{C_E} = \frac{C_s}{C_L} = \frac{C_\sigma}{C_f} = 1 \tag{3}$$

where the symbols L, γ, s, E, ν, σ, ε, f denote the parameters of geometry, density, displacement, deformation modulus, Poisson's ratio, stress, strain and strength. The scale chosen for this model dam is shown in Table 1.

2.1 Material properties

Table 2 summarizes the material properties of the prototype and the model dam. In China, roller compacted concrete (RCC) with a water/cement ratio of 0.45-0.60 and a compressive strength no less than 10-20 MPa after 90 days is widely used for constructing gravity dams (Ministry of Water Resources 2005). For physical models of dams, gypsum, plaster, barite, cement, bentonite, etc are commonly used as similitude materials of concrete (Liu *et al.* 2003a, Harris *et al.* 2000, Tinawi *et*

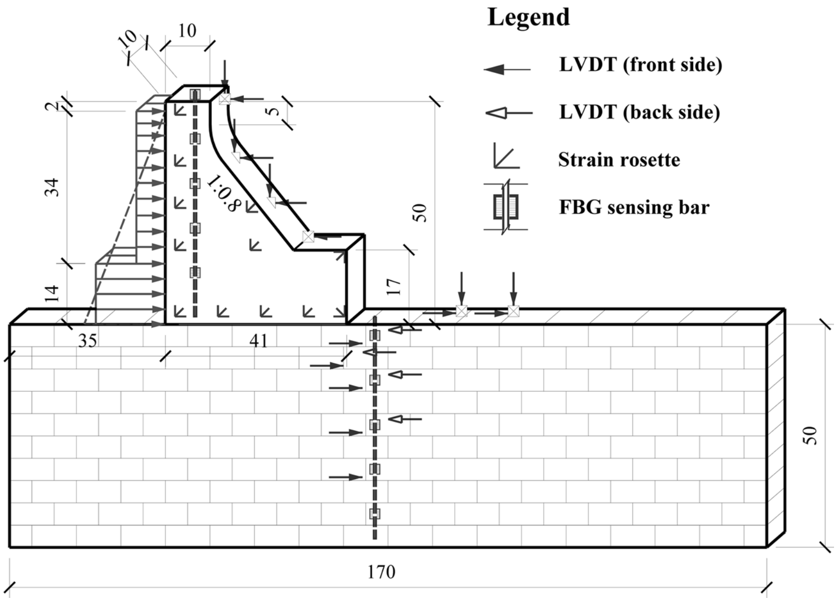

Fig. 1 Model dimensions and instrumentation setup (all dimensions in cm)

Table 1 Similarity coefficients between the prototype and the physical model

Physical parameters	Scale factors	Ratio (prototype/model)
Length	$C_L = \frac{L_p}{L_m}$	150
Density	$C_\gamma = \frac{\gamma_p}{\gamma_m}$	1
Displacement	$C_s = \frac{s_p}{s_m}$	150
Deformation modulus	$C_E = \frac{E_p}{E_m}$	150
Possion's ratio	$C_\nu = \frac{\nu_p}{\nu_m}$	1
Stress	$C_\sigma = \frac{\sigma_p}{\sigma_m}$	150
Strain	$C_\varepsilon = \frac{\varepsilon_p}{\varepsilon_m}$	1
Strength	$C_f = \frac{f_p}{f_m}$	150

The subscripts *p* and *m* denote that the corresponding parameters are of the prototype and the physical models, respectively

Table 2 Properties of the prototype and physical model materials

Material	Property	Prototype	Model
Concrete	Deformation modulus E (MPa)	20000	133
	Poisson's ratio ν	0.2	0.2
	Density γ (kN/m^3)	24	24
	Tensile strength f_t (kN/m^2)	1500	10
	Compressive strength f_c (kN/m^2)	30000	200
Rock	Deformation modulus E (MPa)	8300	55.4
	Poisson's ratio ν	0.3	0.3
	Density γ (kN/m^3)	26	26
	Tensile strength f_t (kN/m^2)	750	5
	Compressive strength f_c (kN/m^2)	7500	50

al. 2000). In this study, the material chosen for simulating the concrete dam body was a mixture of gypsum powder, barite powder, and water. After a series of laboratory tests, the optimal mixture ratio was obtained. The material properties shown in Table 2 satisfy all the similitude requirements of both deformation modulus and strength between the model and the prototype. In laboratory tests, this similitude material was proved to show an elastic behaviour under low stress levels and brittle rupture characteristics at failure like concrete (Chen *et al.* 2006). During model construction, a wood mold was used to produce the precast model of the dam monolith using this material.

Ten layers of prefabricated bricks were constructed to form a regular-jointed rock foundation. The bricks were made of barite powder (as the cementitious material), engine oil and fusible polymer materials (as the admixture). A Y32-50 hydraulic press machine was used to fabricate bricks with a size of 100 mm×100 mm×50 mm (width×height×length). Tight contacts were provided between the boundary of the dam foundation and the steel test frame during model construction. In engineering practice, special attention is paid to the concrete-rock interface of a gravity dam and pressure grouting is frequently used to reinforce the bonding at this interface. Regarding this, the interface between the dam body and the rock foundation in the physical model test was glued by epoxy resin to ensure ideal bonding.

2.2 Test conditions and procedures

During testing, a progressive overloading that simulated the increase of hydrostatic water pressure was loaded on the upstream face of the model dam. With regard to the uplift pressure, as the dam deadweight is offset greatly by its effect, it is one of the critical factors for dam stability. However, various engineering measures such as sheet piling and grouting, are commonly used in the foundation to control the uplift pressure in a safe magnitude. Because the focus of this study is mainly on the overloading response of the dam subjected to increased horizontal loading, the adverse influence of uplift pressures is not considered in the model test.

The hydrostatic pressure was equalized by two servo-controlled hydraulic jacks arranged on the dam body. The lateral loading was applied with an overloading factor (OF) which is the ratio of the applied loading over the normal (design) hydraulic loading on the model dam, i.e.

$$\mathrm{OF} = \frac{\frac{1}{2}\gamma H^2}{\frac{1}{2}\gamma_0 H^2} = \frac{\gamma}{\gamma_0} \tag{4}$$

where γ_0 is the actual density of water, γ is the increased density of water, and H is the dam height. The safety degree of the dam structure can be evaluated in terms of overloading factors (Alonso *et al.* 1996). The entire process of dams developing from elastic state to failure state can be characterized by two overloading factors of safety, i.e., K_1 for initial cracking and K_2 for ultimate failure.

At the beginning of the test, half of the normal hydrostatic load, that is, an overloading factor of 0.5 was applied on the model dam. After the readings of all the instruments became stable, the lateral load was increased gradually with the overloading factors of 0.8, 1.0, 1.2, 1.4, 1.6, … until 7.4 when the dam-foundation system was completely destroyed.

2.3 Instrumentation

Three types of instruments were installed on the dam-foundation system, in order to investigate the deformation mechanism of the model dam under overloading and determine the factors of safety. The instrumentation details are shown in Figs. 1, 2 and 3.

(1) For the dam body, a tension zone indicates the formation of cracks in the concrete while a compression zone may result in crushing of concrete. To measure the magnitudes and directions of the principal stresses, a total of twelve electrical strain rosettes were installed on the dam body.

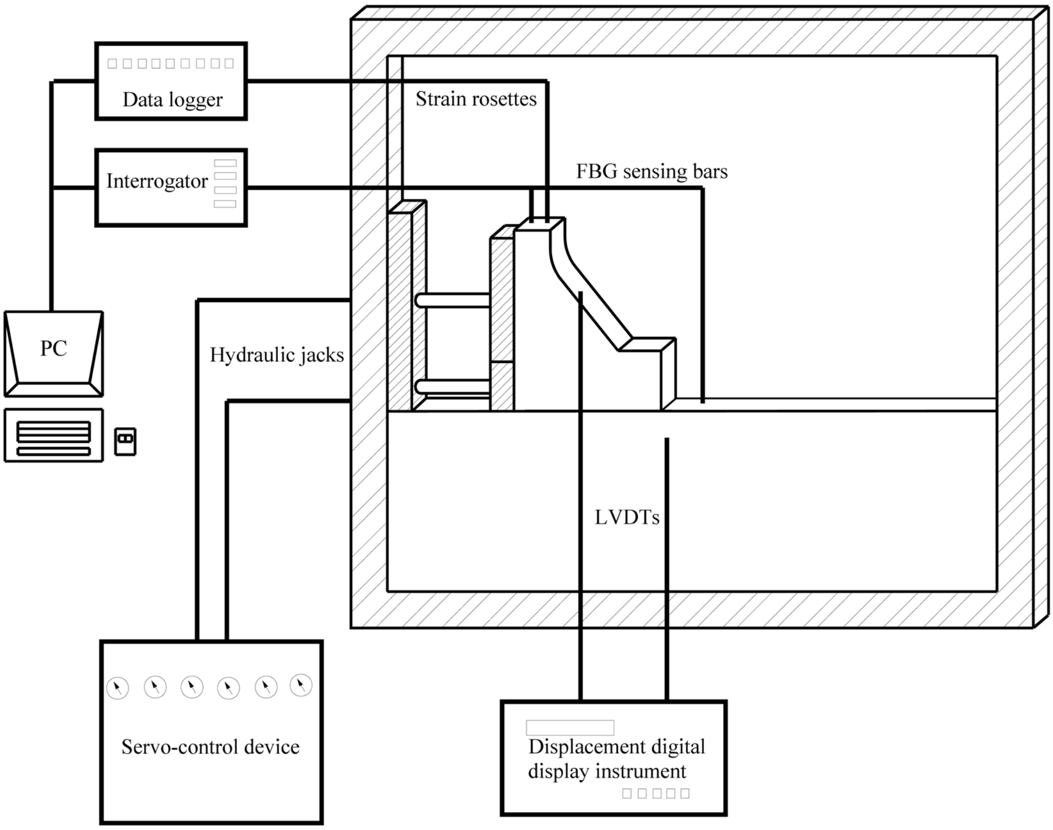

Fig. 2 Loading and measurement system for the physical model test

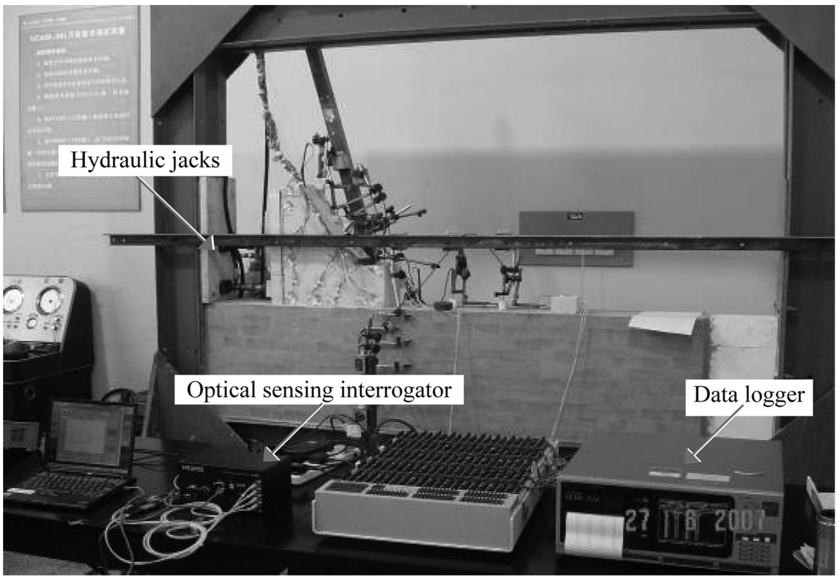

Fig. 3 Photograph of the physical model test (monitoring in progress)

They were connected to a datalogger with full bridge configuration for data acquisition.

(2) For the measurement of surface displacements of the dam body, three horizontal and four vertical linear variable displacement transformers (LVDTs) were installed. The other nine LVDTs were installed below the dam toe for horizontal displacement measurement of the rock foundation. Two pairs of LVDTs were installed on the ground surface and kept a distance from the dam toe for the estimation of displacement influence range. A displacement digital display instrument was utilized to take their measurements.

(3) To monitor internal displacements induced by the overloading, two fiber Bragg grating (FBG) sensing bars were installed inside the model dam. The FBG sensing bar has two series of surface adhered FBG sensors, which measures the strain distributions along the bar. When it is embedded into a physical model and deforms as a result of loading, the displacement profiles in the axial and transverse directions along the sensing bar can be measured based on the strains measured by the quasi-distributed FBG sensors (Zhu *et al.* 2010). It combines the functions of in-place inclinometers and borehole extensometers. The FBG sensing bars used in this test had a diameter of 10 mm and a length of 500 mm. Each bar had ten FBG sensors and the sensor spacing was 100 mm.

Prior to testing, one of the FBG sensing bars was embedded in the dam body to monitor the internal deflection (horizontal displacement) and vertical relative displacement distribution from the dam top to the ground surface. The other FBG sensing bar was embedded in the downstream rock foundation near the dam toe, for monitoring ground settlements and horizontal displacement profiles in the dam foundation. To facilitate the installation, two predefined holes of 14 mm diameter and 500 mm depth were prepared during model construction. The gap between the bars and the holes was grouted with quick-set silicon glue. An optical sensing interrogator was used to record the Bragg wavelengths of the FBG sensing bars in real time.

3. Physical model test results and analysis

3.1 Observation

From zero to normal loading condition, no visible crack of the model dam was detected. The first crack appeared under the dam heel when the lateral loading was increased to an overloading factor of 3.0. This indicated that the shear resistance of the foundation at this location could not sustain the lateral loading any more. Because the dam foundation had regular mortar joints, the main horizontal crack trajectory was found between the first and second brick layers. When the overloading factor was raised to 4.0, crack propagation within the dam foundation became significant and the main vertical cracks at the dam heel developed quickly, showing that the dam foundation gradually lost its bearing capacity. A partial crush zone was seen at the dam toe, where the dam was subjected to compression-shear loading. When loading continued to increase, more and more horizontal cracks appeared in the foundation. When the overloading factor reached 7.4, the main horizontal crack formed completely at the shallow layer, as shown in Fig. 4. The lines visible on the body of the dam in Fig. 4 are the cables of the strain rosettes. The width of the main tension crack below the dam heel has a maximum value of about 6 mm. It was seen that at this moment, the deformation of the dam was mainly due to the horizontal shear sliding of the foundation. No visible damage of the dam body was detected during the whole process of overloading.

From the above observations, the failure of the dam-foundation system was caused by sliding

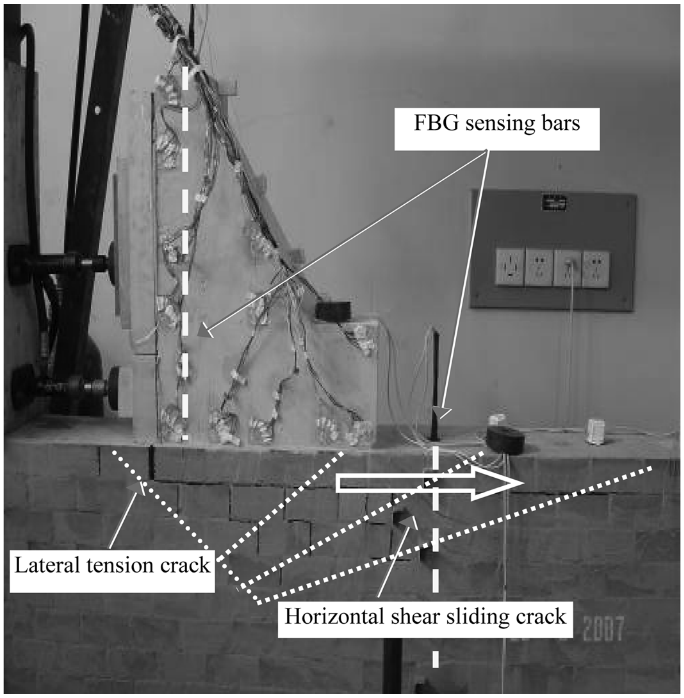

Fig. 4 Photograph of sliding failure of the model dam (OF=7)

within the rock foundation. The overloading factors of safety K_1 and K_2 can be estimated to be around 3 and 4, respectively. The failure mode illustrated that the jointed rock foundation below the heel and the toe were two weak locations and should be given adequate attention in the process of dam design and construction.

3.2 Performance of the dam body

3.2.1 Surface displacements

The surface displacements of the dam body measured by seven LVDTs are shown in Fig. 5. The results reveal a rotation tendency at the dam toe due to the increased upstream pressure. When the overloading factor was between 0 and 1, the overloading factor-displacement curves were approximately linear, indicating an elastic behaviour of the dam-foundation system at this stage. Under the normal loading condition, the maximum horizontal and vertical displacements occurred at the dam crest and had the same value of 0.02 mm (3 mm for prototype). When the overloading factor reached 3.0, abrupt increases of displacement rates were found. The corresponding horizontal and vertical displacements at the dam crest were 0.49 mm and 0.09 mm (73.5 mm and 13.5 mm for prototype). When the lateral loading increased to an overloading factor of 4.0, another turning point of the displacement curves appeared. The measured horizontal displacements developed quickly and reached over 6 mm (900 mm for prototype) at an overloading factor of 5.8. At this stage, the displacements were mainly the horizontal rigid body motion (translation), which was due to the sliding within the rock foundation. This phenomenon is similar to the centrifuge modelling results of unnotched specimens done by Plizzari *et al.* (1995).

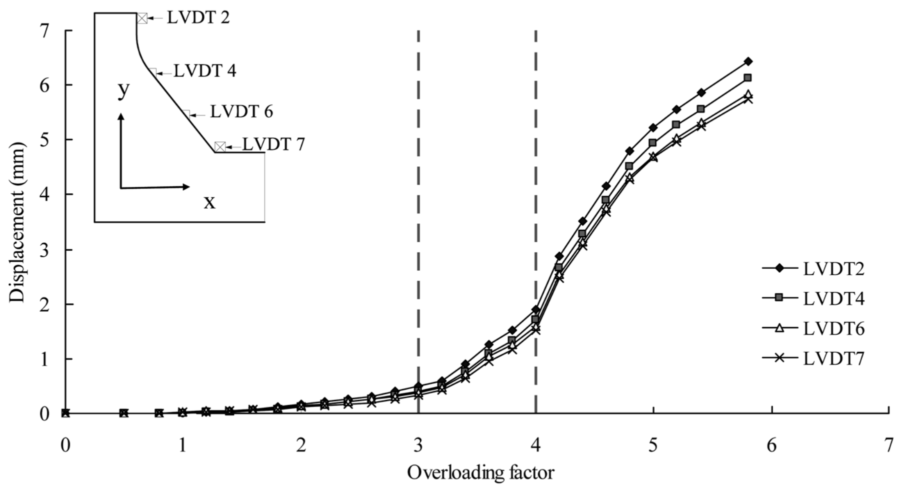

(a) Horizontal displacements of the monitoring points

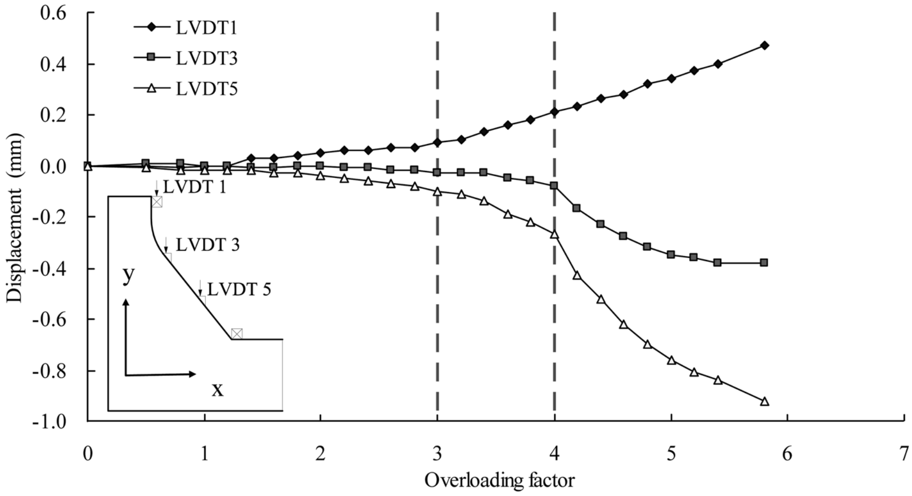

(b) Vertical displacements of the monitoring points

Fig. 5 Surface displacements of the dam body measured by LVDTs during overloading (positive LVDT values for the *x*/*y* directions as shown) (a) Horizontal displacements of the monitoring points; (b) Vertical displacements of the monitoring points

From the quantitative tendencies of the displacements shown in Fig. 5, the cracking overloading factor of safety K_1 and failure factor of safety K_2 can be determined as 3.0 and 4.0 respectively, which is quite consistent with the estimation from observations.

3.2.2 Internal displacements

The displacements of the dam body monitored by the FBG sensing bar are shown in Figs. 6 and 7. The results reveal that the deformation was mainly the deflection of the dam body in the horizontal direction and the maximum displacement occurred at the dam top. At the same time, the upstream dam body was subjected to slight tension in the vertical direction. During the whole

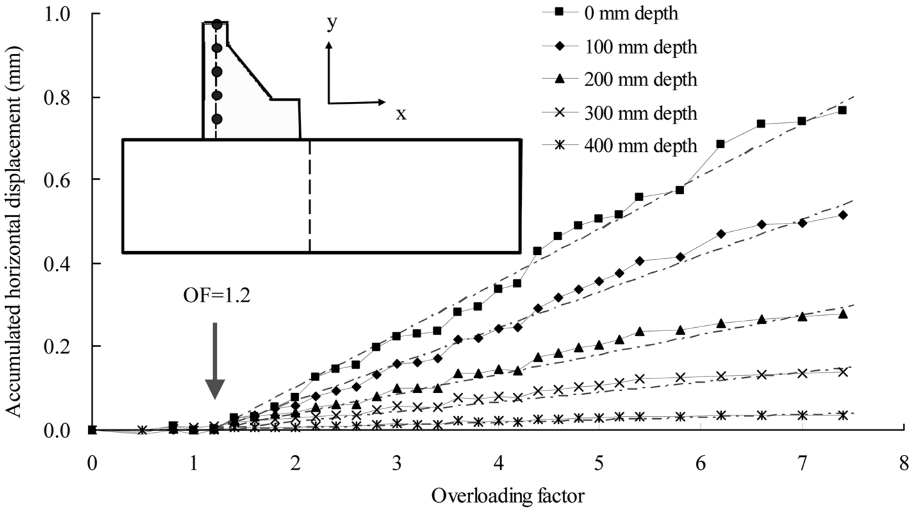

(a) Relationships of overloading factors and accumulated horizontal displacements with respect to ground level at different depths (positive displacements indicate movement of the dam body in the *x* direction)

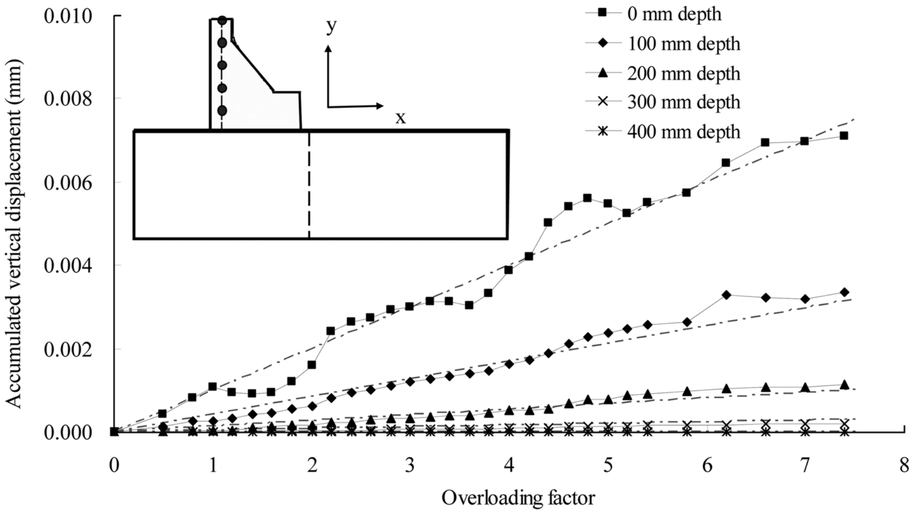

(b) Relationships of overloading factors and accumulated vertical displacement with respect to ground level at different depths (positive displacements indicate tension of the dam body)

Fig. 6 Displacements of the mode dam body measured by the FBG sensing bar (a) Relationships of overloading factors and accumulated horizontal displacements with respect to ground level at different depths (positive displacements indicate movement of the dam body in the *x* direction); (b) Relationships of overloading factors and accumulated vertical displacement with respect to ground level at different depths (positive displacements indicate tension of the dam body)

process of overloading, the dam body was shown to behave linearly (presumably elastically). Under the normal loading condition (OF=1), the maximum horizontal and vertical (relative) displacements inside the dam body near the upstream face were 0.010 mm and 0.001 mm (1.5 mm and 0.15 mm

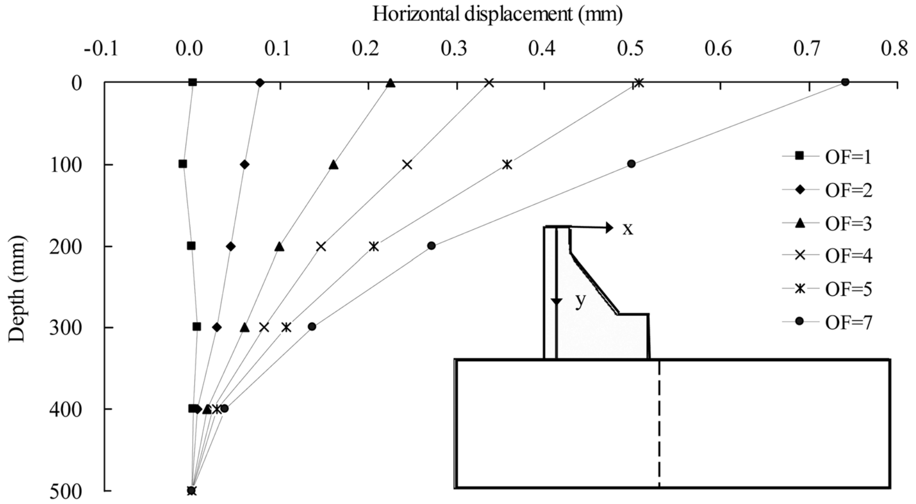

Fig. 7 Profiles of horizontal displacements with respect to depths of the dam body under different overloading

for prototype). At the failure point (OF=4), the horizontal and vertical displacement reached 0.337 mm and 0.004 mm (50.6 mm and 0.6 mm for prototype). The magnitudes of the displacements were considerably small and didn't reflect any stability problem of the dam-foundation system.

3.2.3 Strains and stresses of the dam body

From the strain monitoring results shown in Fig. 8, the strains gradually increased with the increase of lateral loading and a strain concentration was located at the dam heel. For most of the strain rosettes, the overloading factor-strain curves showed approximately linear relationships and the magnitudes of tensile strains were very small. High compressive strains dominated the dam toe but did not exceed the strain limit of the model material during the whole overloading process.

However, the measured strain in the 45^{o} direction at the dam toe demonstrated an abnormal overturning point at an overloading factor of 3.8. This can be considered as a signal that the dam toe turned from compression to tension, which was caused by stress redistribution within the rock foundation. The tensile strain at this point suddenly jumped to over 800 micro strains at an overloading factor of 6.2.

The magnitudes and the directions of the principal stress can be determined by

$$\sigma_{1,2} = \frac{E}{1-\nu}\frac{\varepsilon_0+\varepsilon_{90}}{2} \pm \frac{1}{2}\frac{E}{1+\nu}\sqrt{(\varepsilon_0-\varepsilon_{90})^2+(2\varepsilon_{45}-\varepsilon_0-\varepsilon_{90})^2} \tag{5}$$

$$\tan 2\alpha = \frac{2\varepsilon_{45}-\varepsilon_0-\varepsilon_{90}}{\varepsilon_0-\varepsilon_{90}} \tag{6}$$

where ε_0, ε_{45}, and ε_{90} are the strains in the 0^{o}, 45^{o} and 90^{o} directions; $\sigma_{1,2}$ are the first and second principal stresses; α is the angle between the first principal stress and the 0^{o} direction.

The distribution of principal stresses on the dam body indicated in Fig. 9 show that the internal forces of the dam system automatically adjust under the external loading. Before the occurrence of sliding failure, the dam body behaved elastically without crushing or cracking. Because the dam-

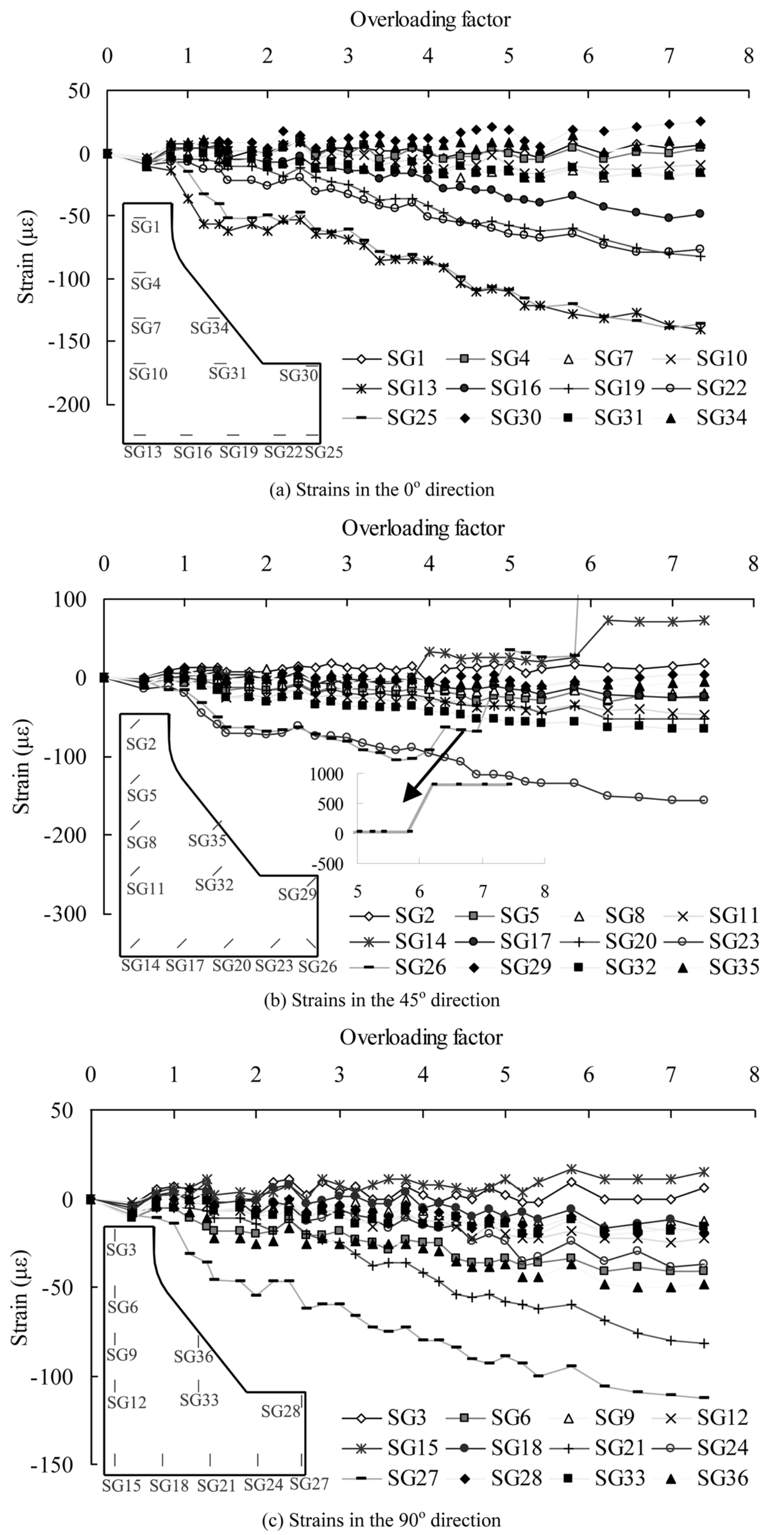

Fig. 8 Strain development on the dam body measured by strain rosettes under overloading condition (strain: "+" for tension and "–" for compression) (a) Strains in the 0° direction; (b) Strains in the 45° direction; (c) Strains in the 90° direction

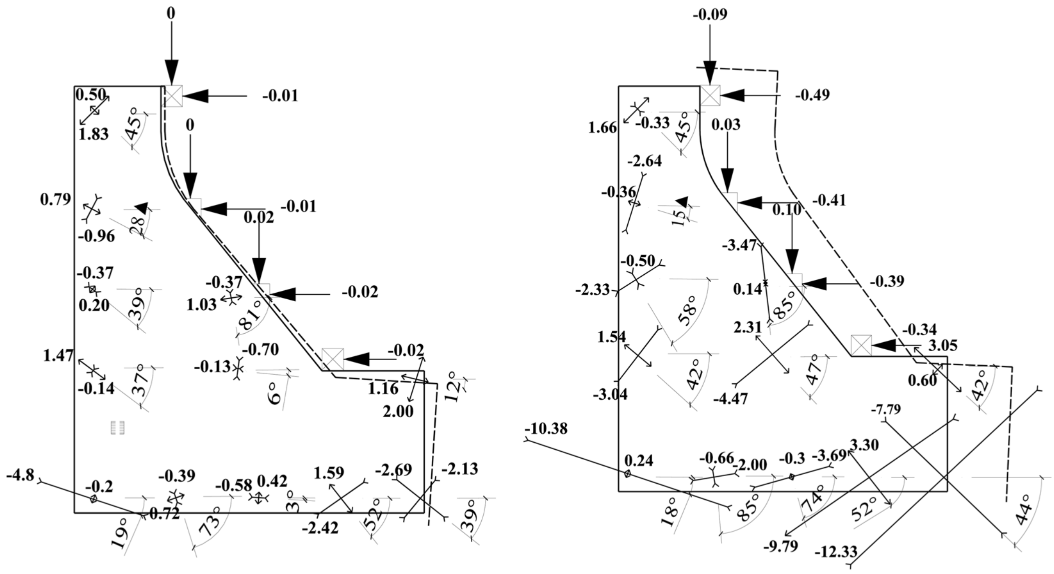

(a) OF=1 (b) OF=3

Fig. 9 Principal stress distributions and surface displacements on the dam body measured by strain rosettes and LVDTs (unit: kPa for stresses, "+" for tension, "–" for compression, mm for displacements, positive LVDT value for the arrow direction as shown) (a) OF=1; (b) OF=3

foundation interface was the essential component that transferred the external overloading to the dam foundation, accumulated strains at this interface were found as expected. The transferred high stresses led to crushing failure below the ground surface.

3.3 Performance of the rock foundation

3.3.1 Surface displacements

The surface displacements of the rock foundation measured by LVDTs are shown in Fig. 10. The horizontal displacement curves measured by LVDT No. 12 and 17 agreed well with the dam body motion shown in Fig. 5(a). Relatively small horizontal displacements were found at the lower part of the rock foundation. The displacements at the ground surface indicated that before cracking of the foundation, the deformation was only localized around the concrete-rock interface. Under the normal loading condition, the maximum horizontal and vertical displacements of the foundation are both 0.02 mm (3 mm for prototype). As soon as sliding of foundation occurred, the region of deformation spread dramatically, especially at the ground surface.

3.3.2 Internal displacements

The horizontal and vertical displacements within the foundation under increased overloading forces are shown in Fig. 11. The maximum horizontal and vertical (relative) displacements occurred 50 mm below the dam toe. Under the normal loading condition (OF=1), the maximum horizontal and vertical (relative) displacements were 0.046 mm and 0.003 mm (6.9 mm and 4.5 mm for prototype). The vertical displacements demonstrated highly nonlinear behaviour. The results show that the rock foundation had subsidence below the dam toe, indicating that this location was

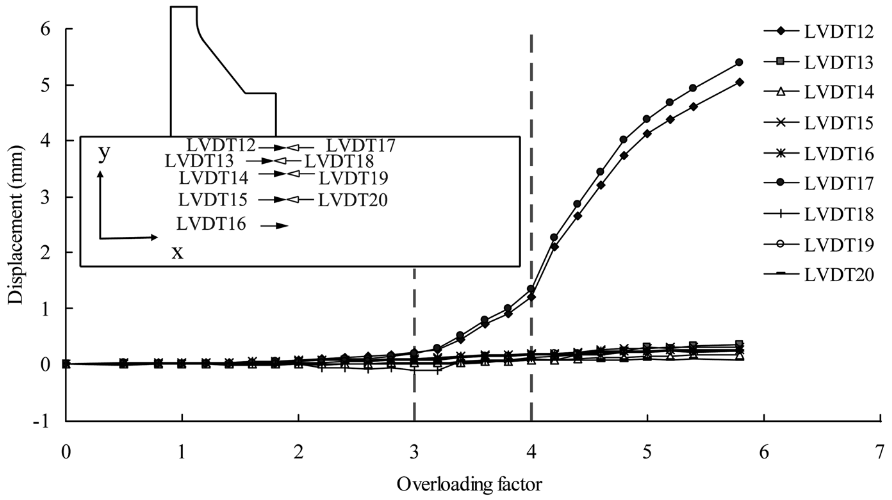

(a) Relationships of overloading factors and horizontal displacements below the ground surface

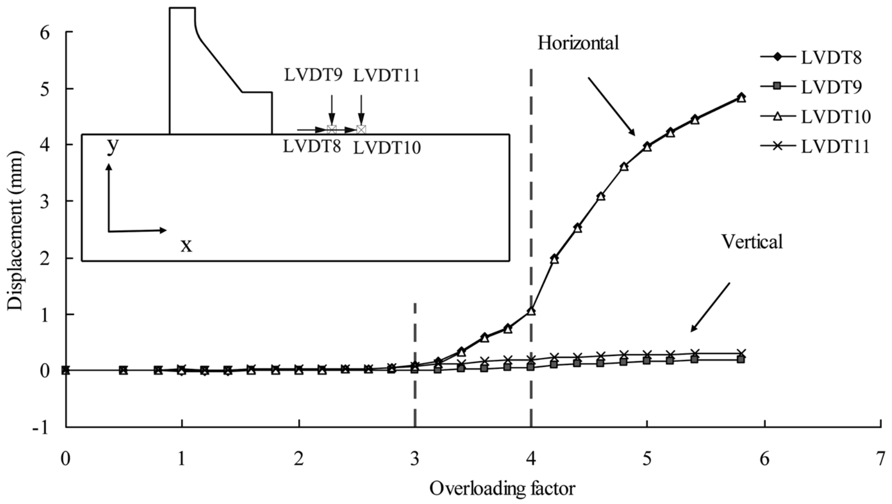

(b) Relationships of overloading factors and ground surface displacements

Fig. 10 Displacements of the dam foundation measured by LVDTs (a) Relationships of overloading factors and horizontal displacements below the ground surface; (b) Relationships of overloading factors and ground surface displacements

subjected to strain concentration. However, there was an obvious turning point of the settlement-overloading curve at OF=4. This can be explained by the fact that the crack penetration resulted in dissipation of energy and therefore slowed down the settlement rates. At this stage, the horizontal and vertical displacement reached 1.313 mm and 0.074 mm (197.0 mm and 11.1 mm for prototype).

From the horizontal displacements shown in Fig. 11(a), the cracking overloading factor of safety K_1 and failure factor of safety K_2 can be also identified to be 3.0 and 4.0 respectively. However, the settlement results in Fig. 11(b) only indicate the ultimate failure of the dam structure.

Fig. 12 demonstrates the horizontal displacement-depth relationship below the dam toe. At the

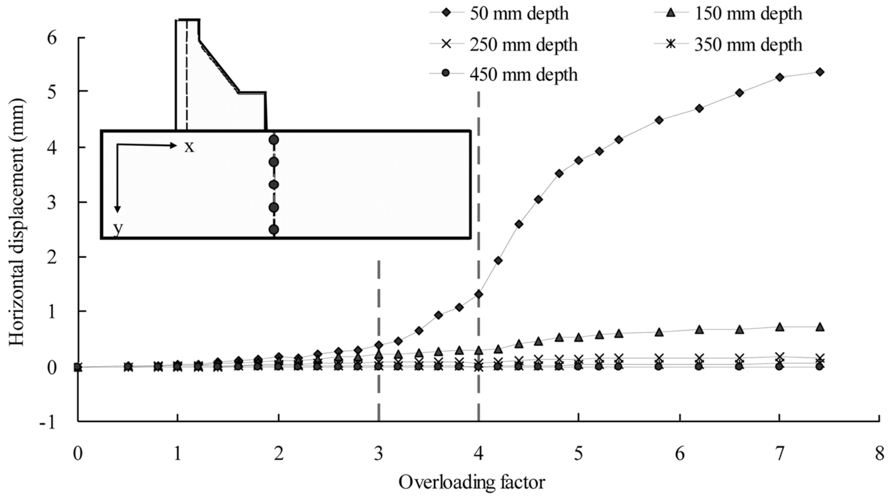

(a) Relationships of overloading factors and relative horizontal displacements

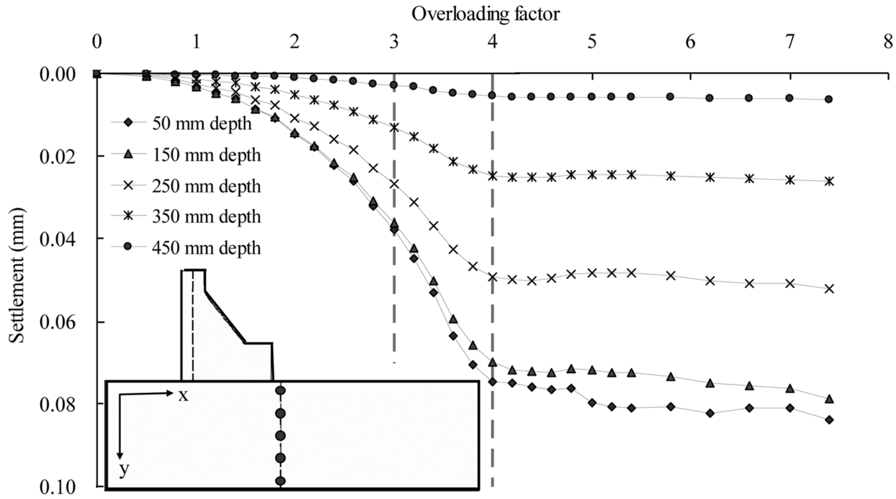

(b) Relationships of overloading factors and settlements (positive settlements indicate compression of the foundation)

Fig. 11 Displacements of the dam foundation measured by the FBG sensing bar (a) Relationships of overloading factors and relative horizontal displacements; (b) Relationships of overloading factors and settlements (positive settlements indicate compression of the foundation)

beginning, the sliding of the rock foundation was seen to be limited to the shallow layer. With the increase of overloading, the ground below the dam was found to slide and shear cracks gradually formed and developed in the horizontal and vertical directions.

3.3.3 Crack propagation and failure pattern

The crack propagation pattern was recorded by a digital camera during overloading. The photographs showed that the cracking was initiated at the base of the upstream side of the dam. During the formation of cracks in the foundation, the strains of the dam body did not undergo any sudden changes. As Ghaemina and Ghobarah (1999) stated, most of the energy input due to the

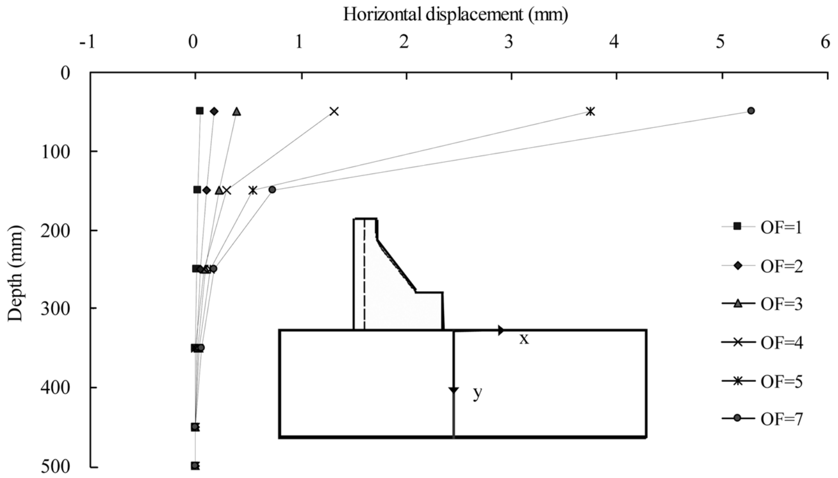

Fig. 12 Profiles of horizontal displacements with respect to depths of the dam foundation under different overloading

increase of hydrostatic loading is dissipated by increased crack width at the heel where the crack was initiated. The ultimate failure pattern is shown in Fig. 4. The visible cracks were located between the joints of the top four layers of bricks. The yield zone can be simplified as a triangle. The increase of overloading was accompanied by a corresponding increase of the height and the vertex angle once the first crack was induced.

4. Conclusions

In this study, a physical model test of a concrete gravity dam on rock foundation was performed under 1g conditions. In the test, the hydrostatic water pressure increased gradually and the uplift forces were not considered. The structural response was captured by various instruments, including strain rosettes, LVDTs and FBG sensing bars. Based on the experimental investigation of the deformation process and failure mechanism of the gravity dam-foundation system, conclusions are obtained as follows:

1. It has been found that physical model tests have unique advantages over other analysis approaches for studying stability related issues of dam structures. In physical model tests, the concrete dam body and the rock foundation with joints and weak layers can be simulated using various similitude materials. The factor of safety can be reasonably defined as the ratio between the maximum external load inducing the start of sliding instability of the dam foundation and the upstream hydrostatic load applied to the dam. Therefore, it gives a convenient and straightforward indication of the foundation resistance against external loads. Moreover, by applying overloading, the captured monitoring results can reveal the potential sliding surfaces and the most critical failure mechanisms. Therefore, this method provides practical guidelines for the design and construction of dam structures.

2. Under overloading conditions, the internal forces of a gravity dam system including the dam body and the rock foundation can automatically adjust. However, the self-adjusting capability of gravity dam system is limited. If enough bonding resistance between the concrete dam body and the rough rock surface is provided, the sliding failure will occur within the rock foundation. As soon as

the external loading exceeds the self-adjusting capability of the gravity dam, localized yield zones will be induced and developed in the foundation, leading to ultimate failure of the dam structure.

3. The results of the physical model tests show that the stability of the gravity dam under investigation is sufficient for the design loading combination. Under the action of the normal working loads, the maximum horizontal displacement of the prototype dam structure will be less than 3 mm. The tension cracks of the overloaded dam initiate under the dam heel and the most critical potential sliding surface lies below the dam-foundation interface. The shear strengths of joints in the rock foundation play a dominant role in determining the dam stability. In addition, the horizontal displacements at the dam toe/crest are the signs of potential failure, which should be paid special attention in dam safety monitoring.

Acknowledgements

The authors gratefully acknowledge the financial support provided by the Open Fund of the State Key Laboratory of Hydraulics and Mountain River Engineering, Sichuan University (No. SKLH-OF-0808) and the National Natural Science Foundation of China (Grant No. 50879050). The development of FBG sensing bars was funded by the grants from The Hong Kong Polytechnic University (Grant Nos. G-YE54 and 1-BB7U).

References

Alonso, E., Carol, I., Delahaye, C., Gens, A. and Prat, P. (1996), "Evaluation of factor of safety in discontinuous rock", *Int. J. Rock Mech. Min.*, **33**(5), 513-537.

ASCE Task Committee on Instrumentation and Monitoring Dam Performance (2000), *Guidelines for Instrumentation and Measurements for Monitoring Dam Performance*, *ASCE*, Reston, VA.

Barpi, F., Ferrara, G., Imperato, L. and Valente, S. (1999), "Lifetime of concrete dam models under constant loads", *Mater. Struct.*, **32**(2), 103-111.

Bhattacharjee, S.S. and Léger, P. (1993), "Seismic cracking and energy dissipation in concrete gravity dams", *Earthq. Eng. Struct. Dyn.*, **22**(11), 991-1007.

Bhattacharjee, S.S. and Léger, P. (1994), "Application of NLFM models to predict cracking in concrete gravity dams", *J. Struct. Eng. - ASCE*, **120**(4), 1255-1271.

Chen, S.H., Li, Y.M., Wang, W.M. and Shahrour, I. (2004), "Analysis of gravity dam on a complicated rock foundation using an adaptive block element method", *J. Geotech. Geoenviron. Eng. - ASCE*, **130**(7), 759-763.

Chen, S.H., Qiang, S., Shahrour, I. and Egger, P. (2008), "Composite element analysis of gravity dam on a complicated rock foundation", *Int. J. Geomech. - ASCE*, **8**(5), 275-284.

Chen, Y., Zhang, L., He, X.S., Chen, J.Y. and Hu, C.Q. (2006), "Evaluation of model similarity of induced joints in a high RCC arch dam", *Proceedings of the 6th Conference of Physical Modeling in Geotechnics*, Hong Kong, 413-417.

Chopra, A.K. and Zhang, L. (1991), "Earthquake-induced base sliding of concrete gravity dams", *J. Struct. Eng. - ASCE*, **117**(12), 3698-3719.

Donlon, W.P. and Hall, J.F. (1991), "Shaking table study of concrete gravity dam monoliths", *Earthq. Eng. Struct. Dyn.*, **20**(8), 769-786.

Ftima, M.B. and Léger, P. (2006), "Seismic stability of cracked concrete dams using rigid block models", *Comput. Struct.*, **84**(28), 1802-1814.

Ghaemina, M. and Ghobarah, A. (1999), "Nonlinear seismic response of concrete gravity dams with dam-reservoir interaction", *Eng. Struct.*, **21**(4), 306-315.

Ghobarah, A. and Ghaemian, M. (1998), "Experimental study of small scale dam models", *J. Eng. Mech. - ASCE*, **124**(11), 1241-1248.
Harris, D.W., Snorteland, N., Dolen, T. and Travers, F. (2000), "Shaking table 2-D models of a concrete gravity dams", *Earthq. Eng. Struct. Dyn.*, **29**(6), 769-787.
Javanmardi, F., Leger, P. and Tinawi, R. (2005), "Seismic water pressure in cracked concrete gravity dams: experimental study and theoretical modeling", *J. Struct. Eng. - ASCE*, **131**(1), 139-150.
Li, Q.S., Li, Z.N., Li, G.Q., Meng, J.F. and Tang, J. (2005b), "Experimental and numerical seismic investigations of the Three Gorges dam", *Eng. Struct.*, **27**, 501-513.
Liu, J., Feng, X.T. and Ding, X.L. (2003b), "Stability assessment of the Three-gorges Dam foundation, China using physical and numerical modelling-Part II. numerical modelling", *Int. J. Rock Mech. Min.*, **40**(5), 633-652.
Liu, J., Feng, X.T., Ding, X.L., Zhang, J. and Yue, D.M. (2003a), "Stability assessment of the Three-gorges Dam foundation, China using physical and numerical modelling-Part I. physical model tests", *Int. J. Rock Mech. Min.*, **40**(5), 609-631.
Mao, M. and Taylor, C.A. (1997), "Non-linear seismic cracking analysis of medium-height concrete gravity dams", *Comput. Struct.*, **64**(5-6), 1197-1204.
Martt, D.F., Shakoor, A. and Greene, B.H. (2005), "Austin Dam, Pennsylvania: the sliding failure of a concrete gravity dam", *Environ. Eng. Geosci.*, **11**(1), 61-72.
Ministry of Water Resources, P.R. China. (2005), *Design Specification for Concrete Gravity Dams (SL319-2005)*, Chinese Water Conservancy and Hydro-electric Power Publishers, Beijing. (in Chinese)
Mir, R.A. and Taylor, C.A. (1996), "An investigation into the base sliding response of rigid concrete gravity dams to dynamic loading", *Earthq. Eng. Struct. Dyn.*, **25**(19), 79-98.
Morin, P.B., Leger, P. and Tinawi, R. (2002), "Seismic behavior of post-tensioned gravity dams: shake table experiments and numerical simulations", *J. Struct. Eng. - ASCE*, **128**(2), 140-152.
Plizzari, G., Waggoner, F. and Saouma, V.E. (1995), "Centrifuge modelling and analysis of concrete gravity dams", *J. Struct. Eng. - ASCE*, **121**(10), 1471-1479.
Ren, X.H., Shu, J.Q., Ben, N.H. and Ren, H.Y. (2008), "Stability analysis of concrete gravity dam on complicated foundation with multiple slide planes", *Water Sci. Eng.*, **1**(3), 65-72.
Rochon-Cyr, M. and Léger, P. (2009), "Shake table sliding response of a gravity dam model including water uplift pressure", *Eng. Struct.*, **31**(8), 1625-1633.
The State Economic and Trade Commission, P.R. China. (2000), *Design Specification for Concrete Gravity Dams (DL5108-1999)*, China Electric Power Press, Beijing. (in Chinese)
Tinawi, R. and Guizani, L. (1994), "Formulation of hydrodynamic pressures in cracks due to earthquakes in concrete dams", *Earthq. Eng. Struct. Dyn.*, **23**(7), 699-715.
Tinawi, R., Leger, P., Leclerc, M. and Cipolla, G. (2000), "Seismic safety of gravity dams: from shake table experiments to numerical analysis", *J. Struct. Eng. - ASCE*, **126**(4), 518-529.
U.S. Army Corps of Engineers. (1995), *Engineering and Design-Gravity Dam Design*, Department of the Army, Washington, D.C.
Xu, Q.J., Li, X. and Chen, Z.Y. (2007), "Three-dimensional stability analysis of the dam foundation at Baise", *Front. Archit. Civil. Eng. China*, **1**(2), 217-221.
Yan, F.Z., Tu, X.B. and Li, G.C. (2004), "The uplift mechanism of the rock masses around the Jiangya dam after reservoir inundation", *China Eng. Geology*, **76**, 141-154.
Zhang, C.H., Wang, G.L., Wang, S.M. and Dong, Y.X. (2002), "Experimental tests of rolled compacted concrete and nonlinear fracture analysis of rolled compacted concrete dams", *J. Mater. Civil. Eng.*, **14**(2), 108-115.
Zhou, W., Chang, X.L., Zhou, C.B. and Liu, X.H. (2008), "Failure analysis of high-concrete gravity dam based on strength reserve factor method", *Comput. Geotech.*, **35**(4), 627-636.
Zhu, H.H., Yin, J.H., Zhang, L., Jin, W. and Dong, J.H. (2010), "Monitoring internal displacements of a model dam using FBG sensing bars", *Adv. Struct. Eng.* (in press)
Zhu, X.Y. and Pekau, O.A. (2007), "Seismic behavior of concrete gravity dams with penetrated cracks and equivalent impact damping", *Eng. Struct.*, **29**, 336-345.

PL